First principles determination of static, dynamic and electronic properties of some liquid 4d transition metals near melting

Luis E. González [*], David J. González

Departamento de F sica Teórica, Universidad de Valladolid, 47011 Valladolid, Spain.

ARTICLE INFO

ABSTRACT

The static and dynamic properties of several bulk liquid 4d transition metals at thermodynamic conditions near their respective melting points have been evaluated by using *ab-initio* molecular dynamics simulations. The calculated static structure factors show an asymmetric second peak followed by a more or less marked shoulder which points to a sizeable amount of icosahedral local order. Special attention is devoted to the analysis of the obtained longitudinal and transverse current spectral functions and the corresponding dispersion of collective excitations. For some metals, we have found the existence of two branches of transverse collective excitations in the second pseudo-Brillouin zone. Finally, results are also reported for several transport coefficients.

1. Introduction

This paper reports an *ab initio* molecular dynamics (AIMD) simulation study of the static, dynamic and electronic properties of several liquid 4d transition metals (Y, Zr, Nb, Mo, Ru and Rh) at thermodynamic conditions near melting.

These metals (with the exception of Ytrium) have usually been included within the group of the so-called refractory metals which are a class of materials characterized by a very high melting temperature ($\geq$ 1850 °C). Refractory metals and alloys have attracted much attention because of their remarkable properties such as resistance to high heat, corrosion and wear. Practical applications include casting molds, wire filaments, reactant vessels for corrosive materials, hard tooling, and several other applications where high density is desired. Furthermore, as these metals possess extraordinary high-temperature properties, they are also strong candidates for high-temperature applications such as structural materials for fission reactors and first wall, blanket, and divertor materials for fusion reactors. Consequently, their great technological interest underlies the importance of the research concerning a better understanding of their structural, dynamical and electronic properties.

In the specific case of the molten state, the fact that these metals have high melting temperatures combined with a high reactivity poses important challenges when trying to measure their liquid state properties. But a good understanding of their thermophysical properties is important for studies on phase transformations, nucleation, atomic dynamics and surface physics as well as industrial processes (*i.e.* refining, casting and welding) and for designing alloys.

Surprisingly, the technological relevance of these metals has not been correlated with the availability of experimental data concerning its molten state structural, dynamic and electronic properties. Information about the structural short-range order in a liquid system can be extracted from the static structure factor, $S(q)$ and/or the pair distribution function, $g(r)$. In the case of the above mentioned liquid 4d metals, there are experimental structural data for liquid Zr (l-Zr) and l-Rh only. For l-Zr, the $S(q)$ was first measured by X-ray diffraction (XD) experiments carried out by Waseda *et al* [1,2] about fifty years ago. More recently, Schenk *et al* [3] have used neutron diffraction (ND) to measure the $S(q)$, yielding results similar to the earlier XD ones although with some differences concerning the amplitude of the oscillations. In the case of l-Rh, Filipponi *et al* [4] have used the X-ray absortion fine structure (XAFS) technique to determine the shape of the first peak of the pair distribution function, $g(r)$.

As for the dynamical properties, very few magnitudes have been measured and those refer to their transport coefficients only. In the case of the 4d metals considered in this paper, their shear viscosities have been measured by means of levitation techniques [5–9]; however, their diffusion coefficients have not been determined yet and the adiabatic sound velocity has only been measured for l-Mo [10].

This lack of data concerning the different physical properties of these liquid metals is a consequence of the difficulties inherent to the process of performing measurements at those high melting temperatures.

---

* Corresponding author.
E-mail addresses: luisen@metodos.fam.cie.uva.es (L.E. González), david@metodos.fam.cie.uva.es (D.J. González).

Therefore, it is important to use other approaches such as theoretical/computer simulation methods in order to extract information about their static, dynamic and electronic properties in the molten state.

However, few theoretical studies, either based on semiempirical or more fundamental methods, have been dedicated to the study of these liquid 4d transition metals and these have mainly focused on thermodynamic and static structural properties. Jakse and Pasturel [11,48] have performed AIMD simulations of l-Zr in order to analyze the local order and its evolution upon undercooling. Their calculated static structure was found to be in very good agreement with the measurements of Schenk *et al* [3]. More recently, Su *et al* [9] have investigated the static structure and the temperature dependence viscosity of stable and undercooled Zr by using levitation techniques and classical molecular dynamics (CMD) simulations. These simulations were performed using a potential derived within the embedded atom method and a cubic supercell with 16,000 Zr atoms. Debela *et al* [12] carried out an AIMD simulation study about the structural evolution of l-Nb during solidification and they evaluated several structural magnitudes. A main conclusion was that the five-fold icosahedral symmetry dominates the local atomic structures in both the liquid and undercooled states. Liquid Mo has also attracted some theoretical studies and, among those, we mention the AIMD simulation study of Belonoshko *et al* [13] about the melting curve of the body centerd cubic phase of Mo over a wide pressure range; moreover for some states they also evaluated some liquid structural magnitudes such as the $g(r)$ and the number of nearest neighbors. More recently, Minakov *et al* [14] have also used AIMD simulations to evaluate several thermophysical properties of l-Mo in the near critical region; more specifically they reported an estimate of the critical point as well as other thermophysical magnitudes of the liquid state such as heat capacities and speed of sound.

This paper reports a molecular dynamics simulation study on a variety of static, dynamic and electronic properties of a group of 4d metals at thermodynamic conditions near their respective melting points. This study has been performed with an AIMD simulation method based on density functional theory (DFT) [15,49], and the liquid metal is modelled as an interacting system of ions and electrons. For a given ionic configuration, DFT allows to find the ground state electronic energy and, *via* the Hellmann-Feynman theorem, the forces acting on the ions whose positions evolve according to classical mechanics while the electronic subsystem follows adiabatically. The AIMD simulation methods involve large computational capabilities and impose some limitations concerning the simulation times and size of the systems under study; however, these drawbacks are somewhat balanced by the accuracy of the delivered results.

Moroeover, there are also other theoretical aspects of current interest which we have also investigated in this paper. This interest has been prompted by the recent finding in some liquid metals of some unusual dynamical features such as transverse low-energy excitations in the dynamic strucure factor [16–18], and/or the appearance of a second, high-frequency peak, in the transverse current spectral functions [19–24,50,51,64]. Furthemore, the existence of this high-frequency peak has recenly been related to the appearance of a second high frequency peak/shoulder in the spectra of the velocity autocorrelation function [22–24,51,64].

There is still a lack of understanding concerning the dynamical processes behind the emergence of the those features as well as the scope of its existence in the liquid metals. Therefore we have also analized the possibe existence of those features in the 4d liquid metals.

The paper has been structured as follows: next section summarizes the basic ideas underlying the AIMD simulation method along with some technical details. In Section 3 we report the results of the calculations which are compared with the available experimental data along with some discussion on them. Finally, a brief summary and conclusions are given in Section 4.

2. Computational method

The AIMD simulations have been performed for l-Y, l-Zr, l-Nb, l-Mo, l-Ru and l-Rh at the thermodynamic states given in Table 1 and by using a cubic cell with 100 atoms (110 atoms for l-Zr).

These AIMD simulations were performed with the DFT based Quantum-ESPRESSO (QE) package [25,52]. The electronic exchange-correlation energy has been described by the generalized gradient approximation of Perdew-Burke-Ernzerhof [26] (Perdew and Wang [27] for l-Zr), including non-linear core corrections. The ion-electron interaction has been described by means of an ultrasoft pseudopotential [28], which was generated from a scalar-relativistic calculation, and Table 1 gives, for each metal, the number of valence electrons explicitly considered in the calculation.

In all cases, the initial atomic positions within the cell were taken at random and the system was thermalized during 5–10 ps of simulation time at the target temperatures listed in Table 1, using the velocity scaling algorithm included in the QE package. Therefrom, after the energy fluctuates around a constant value, microcanonical AIMD simulations at that constant energy were performed, with a timestep of 0.0045 ps, over a number of configurations as given in Table 1. We applied a plane-wave representation with an energy cutoff within the range 25.0–35.0 Ryd. and the single Γ point was used for sampling the Brillouin zone. The number of equilibrium configurations listed in Table 1 were those employed for the evaluation of the static and dynamic properties of the corresponding liquid metal. The structural functions and the mean squared atomic displacements (see results below) were used to assess that the system was indeed in its liquid state (disordered and showing a clear diffusive character, respectively).

Finally, we remark that this simulation method has already provided an accurate description of several static, dynamic and transport properties of other bulk liquid metals [29–31,53–57,65].

3. Results and discussion

3.1. Static properties

The obtained results for the respective static structure factors, $S(q)$, are plotted in Fig. 1. However, comparison with experiment is only available for l-Zr and we observe a good agreement with both the XD data of Waseda *et al* [1,2] and the more recent NS data by Schenk *et al* [3]. Indeed, the comparison is much better with the NS data and this is more visible in the second peak for which the AIMD results predict an asymmetric shape followed by a weak shoulder. This asymmetry of the second peak is found, more or less marked, in the present AIMD results for all the other 4d metals. Although there are no experimental data to compare with, we notice that shoulders on the high-q side of the second peak of $S(q)$ have also been experimentally found in other transition metals (Ti, Fe, Ni) [3,32] and they have been correlated with a significant appearance of icosahedral local order in the liquid. It is found that along the 4d row, from Y to Rh, the height of the main peak takes values within the range 2.70–2.90, while its position, q_p, increases from 2.77

Table 1

Thermodynamic input data of the liquid 4d transition metals studied in the present AIMD simulation study. ρ, is the total ionic number density, (taken from Ref. [10]), T is the temperature, N_{part} is the number of particles in the simulation cell, Z_{val} is the number of valence electrons and N_c is the total number of configurations.

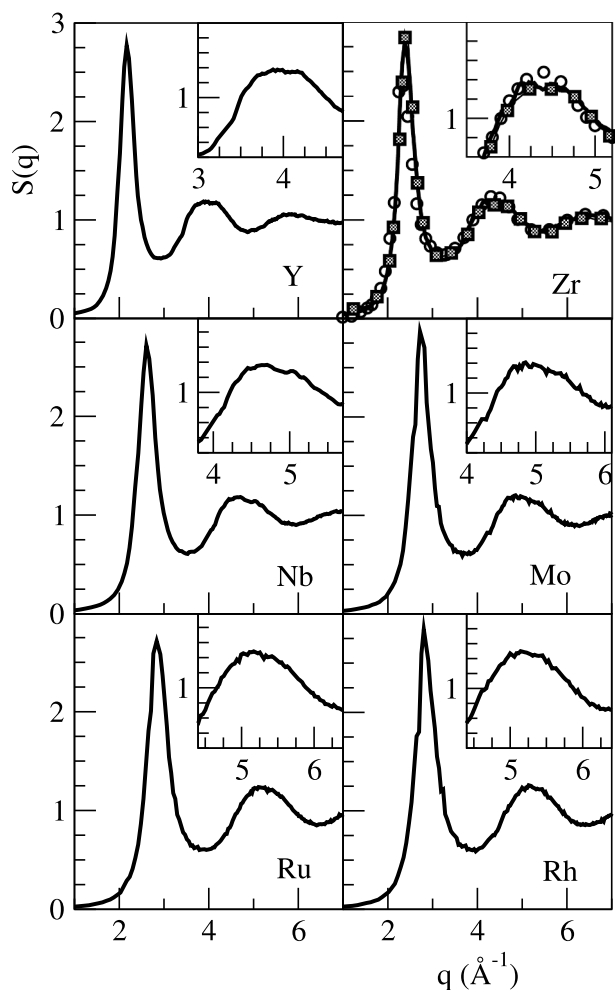|	ρ (Å^{-3})	T (K)	N_{part}	Z_{val}	N_c
Y	0.0287	1850	100	11	11,800
Zr	0.0392	2150	110	12	17,400
Nb	0.0500	2800	100	13	11,500
Mo	0.0578	2950	100	14	10,000
Ru	0.0641	2650	100	16	11,100
Rh	0.0632	2300	100	17	10,100

Fig. 1. Static structure factor, $S(q)$, for several 4d transition metals. Continuous line: present AIMD calculations. The open circles and squares in l-Zr are the XD and ND data of Waseda *et al* [1,2] and Schenk *et al* [3] respectively. The inset shows a closer view of the second maximum.

Å^{-1} (Y) to 2.85 Å^{-1} (Ru, Rh). These values correlate with the changes in number density, and in fact when the $S(q)$ are plotted *vs* a reduced wavelength scaled in terms of the density (see Fig. 2), all the elements fall on an almost universal curve, except for the behavior of the second
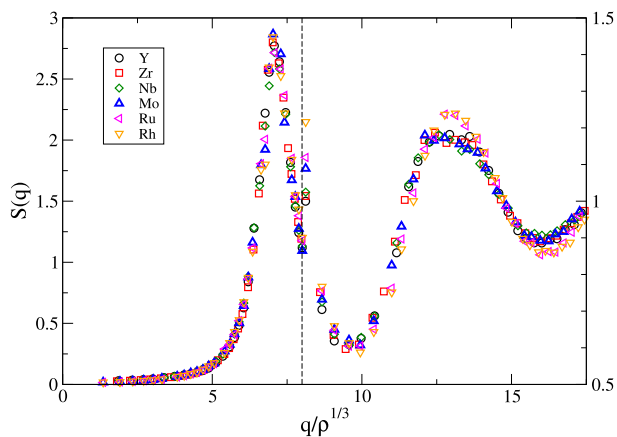

Fig. 2. AIMD calculated static structure factor, $S(q)$, for several 4d transition metals, *vs* reduced wavevector. The oscillations for $q > 8\rho^{1/3}$ have been magnified by a factor of 3.

peak, where Ru and Rh show a common and somewhat more symmetric shape as compared with the rest of systems.

Using the calculated values of $S(q)$, within the range $q \leq 1.2 \text{ Å}^{-1}$, we have obtained an approximate assessment of $S(q \rightarrow 0)$ by using a least squares fit $S(q) = s_0 + s_2 q^2$, yielding the results given in Table 2. Then, the relation $S(q \rightarrow 0) = \rho k_B T \kappa_T$, where k_B is Boltzmann's constant, allows to determine the associated isothermal compressibility, κ_T, and the obtained results are listed in Table 2. We are nor aware of experimental data for κ_T, but for the sake of completeness we have included the values derived by Marcus [33] by using semiempirical expressions which include measured and/or estimated values of several other thermophysical magnitudes.

The pair distribution function, $g(r)$, gives information about the short range order in the liquid and in Fig. 3 we have depicted the calculated AIMD results along with the available experimental data. For l-Zr, the agreement with the NS data of Schenk *et al* [3] is again superior to that with the XD data of Waseda *et al* [1,2]. In the case of l-Rh, we can compare with the XAFS data of Filipponi *et al* [4] which only cover the first peak region showing an excellent agreement with the AIMD results. An evaluation of the number of nearest neighbors or coordination number (CN) has been made by integrating the radial distribution function, $4\pi\rho r^2 g(r)$, up to the position of its first minimum, $r_{\min}$. The results, which are given in Table 2, are typical of simple liquid metals near melting [34].

The common neighbor analysis [35,58] (CNA) method provides a detailed three-dimensional description of the short range order in these liquid metals; more specifically it gives information about the atoms/ions which surround each pair of atoms/ions contributing to the peaks of the $g(r)$. The CNA method discriminates among various local structures like like fcc, hcp,bcc, and icosahedral environments. Different types of pairs are associated to different types of local order. For example, the fcc order only has 1421-type pairs, the hcp structure has the same number of 1421 and 1422-type pairs, the bcc order has six 1441-types pairs and eight 1661 type-pairs and the 13-atom icosahedron (ico) has twelve 1551 type-pairs. The deformation of the regular 1551-type structure, *i.e.* when a bond is broken, yields the 1541 and 1431-type pairs and therefore their presence points to the existence of distorted icosahedral order. For more details about the practical implementation of the CNA method we refer to References [31,57, 35,58].

We have performed a CNA calculation for the 4d metals considered in this study and the results are summarized in Table 3 and Fig. 4. For all the metals, the greatest contribution comes from the 1551-type pairs ranging from 39% (l-Y) to 23% (l-Ru, l-Rh) If we now include the contribution from the 1541 and 1431-type pairs, which are deformed fivefold structures, we conclude that the five-fold symmetry dominates in all these liquid metals as its proportion ranges between $\approx 70\%$ (l-Nb) and $\approx 62\%$ (l-Rh) of the pairs. Note that both l-Ru and l-Rh are the two liquid metals among those studied here that show a very weak shoulder in the second peak of their respective $S(q)$. There is also a significant amount of local bcc-type pairs which range from $\approx 26\%$ (l-Y) to $\approx 11\%$ (l-Ru) of the pairs. Finally, we observe that for l-Ru and l-Rh there is also a noticeable contribution ($\approx 12\%$) from the fcc/hcp type pairs. It is

Table 2

Calculated values for $r_{\min}$ (in Å), position of the first minimum of $r^2 g(r)$), coordination numbers CN, $S(q \rightarrow 0)$ and isothermal compressibilities κ_T (in 10^{-11} m^2 N^{-1} units) for the liquid 4d transition metals at the thermodynamic states given in Table 1. The numbers in parenthesis are semiempirical estimates from Marcus [33].

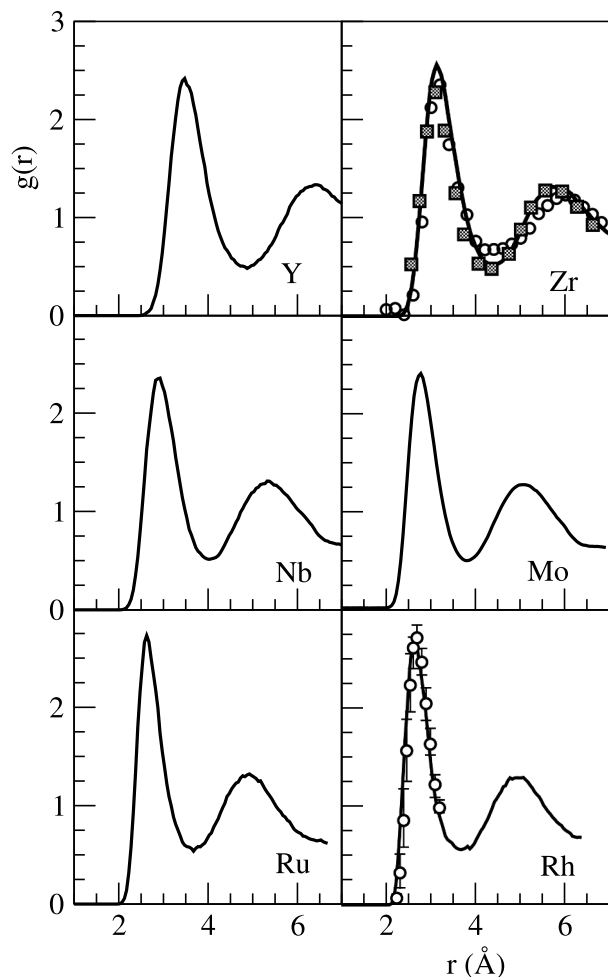|	$r_{\min}$	CN	$S(q \rightarrow 0)$	κ_T
Y	4.72	12.4	0.023 ± 0.002	3.10 ± 0.10 (3.96)
Zr	4.30	13.0	0.017 ± 0.002	1.45 ± 0.15 (1.89)
Nb	3.90	12.8	0.015 ± 0.002	0.78 ± 0.10 (1.23)
Mo	3.73	12.7	0.011 ± 0.001	0.47 ± 0.05 (0.77)
Ru	3.57	12.4	0.012 ± 0.001	0.52 ± 0.05 (1.01)
Rh	3.57	12.4	0.012 ± 0.001	0.60 ± 0.05 (1.05)

Fig. 3. Pair distribution function, $g(r)$, for several 4d transition metals. Continuous line: present AIMD calculations. The open circles and squares in l-Zr are the XD and ND data of Waseda et al. [1,2] and Schenk *et al* [3] respectively. The open circles with error bars in l-Rh are the XAFS data of Filipponi et al. [4].

Table 3
Common neighbor analysis of the AIMD configurations obtained for the liquid 4d transition metals at the thermodynamic states given in Table 1. For comparison we include the values for some common local structures.

	1551	1541	1431	1421	1422	1441	1661
Y	0.39	0.18	0.12	0.01	0.03	0.10	0.16
Zr	0.37	0.18	0.12	0.01	0.02	0.08	0.13
Nb	0.38	0.18	0.14	0.01	0.03	0.07	0.12
Mo	0.25	0.21	0.20	0.03	0.05	0.07	0.11
Ru	0.23	0.21	0.20	0.03	0.06	0.07	0.09
Rh	0.23	0.19	0.20	0.03	0.05	0.07	0.09
hcp	0.0	0.0	0.0	0.50	0.50	0.0	0.0
fcc	0.0	0.0	0.0	1.0	0.0	0.0	0.0
bcc	0.0	0.0	0.0	0.0	0.0	0.43	0.57

worth mentioning that Zr, Nb and Mo melt from a bcc phase, whereas Y, Ru and Rh melt from close-packed structures. Consequently the case of liquid Y is quite special, since it shows the largest amount of bcc local structures among the systems studied here, while the solid bcc phase does not appear at all in its phase diagram, not even at elevated pressures.

3.2. Dynamic properties

We have evaluated several dynamic properties and transport
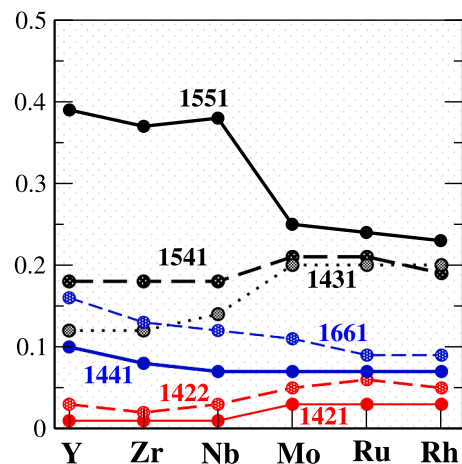

Fig. 4. Variation of the most abundant bonded pairs.

coefficients. These include single-particle magnitudes, such as velocity autocorrelation functions and diffusion coefficients, and also collective properties, such as intermediate scattering functions, longitudinal and transverse current correlation functions and their spectra, sound velocities and shear viscosities.

3.2.1. Single particle dynamics

The (normalized) velocity autocorrelation function (VACF) of a tagged ion in the fluid, $Z(t)$, is defined as

$$Z(t) = \langle \mathbf{v}_1(t) \cdot \mathbf{v}_1(0) \rangle / \langle v_1^2 \rangle \tag{1}$$

with $\mathbf{v}_1(t)$ being the velocity of a tagged ion in the fluid at time t and $\langle \ldots \rangle$ stands for the ensemble average.

The AIMD results for $Z(t)$ are plotted in Fig. 5 where we observe the typical decaying behavior with a pronounced first minimum followed by relatively weak oscillations that damp around zero at longer times. This first minimum appears because of the so-called "cage effect" by which the atom/ion rebounds against the cage formed by its nearest neighbors which induces a vibrational motion at very short times. When going from Y to Rh, the position of the first minimum moves to shorter times because of the increasing number density. The frequency of this vibratory motion can be estimated by a short time expansion $Z(t) = 1 - \omega_E^2/2 + \ldots$, where ω_E is Einstein's frequency of the system; by this procedure we have obtained the following values for ω_E (in ps^{-1}): 19.2 (l-Y), 21.6 (l-Zr), 25.2 (l-Nb), 29.8 (l-Mo), 33.1 (l-Ru) and 31.9 (l-Rh). The Fourier Transform (FT) of $Z(t)$ into the frequency domain gives the associated power spectra, $Z(\omega)$, also known as the vibrational density of states (VDOS). We mention that all the frequency-dependent functions reported in this paper have been obtained by numerical FT of the AIMD obtained time-dependent functions and in this calculation we have used a window function so to reduce the statistical noise present for long times.

The calculated $Z(\omega)$ are plotted as insets in Fig. 5 and we notice that their shapes may display just a peak (l-Y) or a peak followed by a more/less marked shoulder (l-Zr, l-Nb, l-Mo, l-Ru and l-Rh). Analogous results were obtained in a previous AIMD study of several 3d liquid metals [31,57]. It has been recently suggested a connection between the existence of a high frequency shoulder/peak and the appearance (in the transverse dispersion relation) of a second high-frequency transverse branch with practically the same frequency as that of the peak/shoulder [22,51,23]. This feature was found in AIMD studies of l-Zn, l-Sn and l-Tl, and we have corroborated it in the case of some 3d liquid transition metals. We will return to this point in the following section when we present our calculated results in connection with the transverse currents.

The self-diffusion coefficient, D, has been calculated by both the time integral of $Z(t)$ and from the slope of the mean square displacement
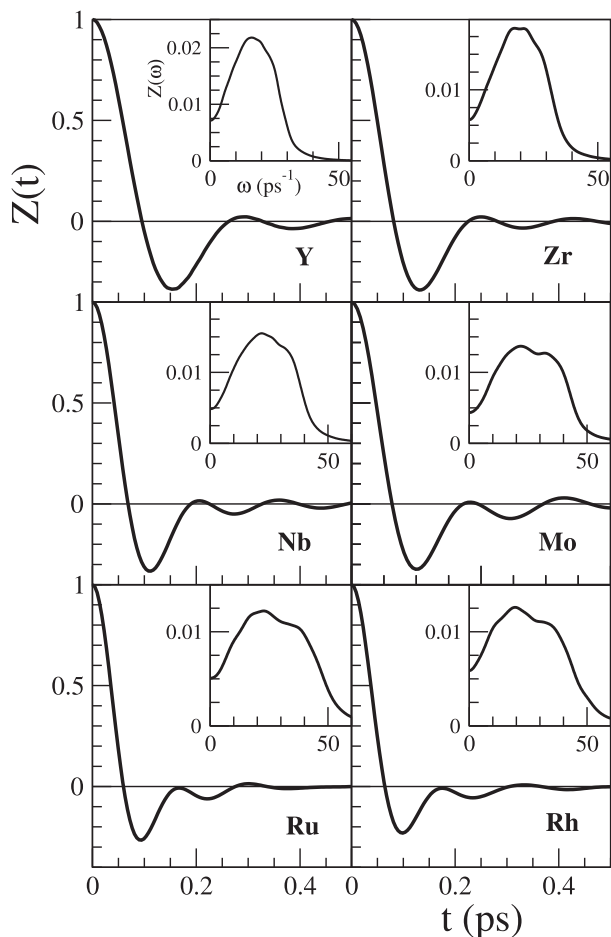
Fig. 5. Normalized AIMD calculated velocity autocorrelation function of several 4d transition metals. The inset represents the corresponding power spectrum $Z(\omega)$.

$\delta R^2(t) \equiv \left\langle \left| \vec{R}_1(t) - \vec{R}_1(0) \right|^2 \right\rangle$ of a tagged ion in the fluid, as follows

$$D = \frac{1}{\beta m} \int_0^\infty Z(t)dt \; ; \quad D = \lim_{t\to\infty} \frac{1}{6} \frac{d\delta R^2(t)}{dt}, \quad (2)$$

where $\beta = (k_B T)^{-1}$ and m is the atomic mass. Both routes yield to practically the same results, which are given in Table 4. Interestingly,

Table 4
Calculated values of the self-diffusion coefficient (D), adiabatic sound velocity (c_s) and shear viscosity (η) for the liquid 4d transition metals at the thermodynamic states given in Table 1.

	D (Å^2/ps)	c_s (m/s)	η (GPa ps)
Y	0.378 ± 0.015	3050 ± 150	3.10 ± 0.20
	0.394 [10]	3143, 3258 [36,59]	2.8 [5]
Zr	0.352 ± 0.015	3450 ± 150	3.80 ± 0.20
	0.383 [10]	3666, 3648 [36,59]	4.5[6]
			3.5[37]
Nb	0.387 ± 0.015	3800 ± 150	5.30 ± 0.20
	0.586 [10]	3593, 3385 [36,59]	4.8 [7]
Mo	0.343 ± 0.015	4400 ± 200	5.70 ± 0.30
	0.520 [10]	4502 [10]	5.0 [8]
Ru	0.355 ± 0.015	4150 ± 200	5.30 ± 0.25
	0.445 [10]	3563, 3214 [36,59]	5.0 [7]
			6.1 [38]
Rh	0.352 ± 0.015	4000 ± 200	5.10 ± 0.25
	0.462 [10]	3283, 2950 [36,59]	4.9 [7]
			5.0–6.1 [39]

the obtained results are very similar for all the 4d metals considered in this work but, unfortunately, there are no experimental data for the self-diffusion coefficient of any of these liquid metals. Nevertheless, we have included in Table 4 some estimates obtained from some semi-empirical expressions, based on a modified Stokes-Einstein formula, which relates the self-diffusion coefficient to other thermophysical magnitudes such as the density and viscosity [10].

3.2.2. Collective dynamics

The intermediate scattering function, $F(q,t)$, provides information about the dynamics of density fluctuations in a liquid. It has been calculated from its definition as.

$$F(q,t) = \frac{1}{N} \left\langle \left(\sum_{j=1}^N e^{-i\mathbf{q}\cdot\mathbf{R}_j(t+t_0)} \right) \left(\sum_{l=1}^N e^{i\mathbf{q}\cdot\mathbf{R}_l(t_0)} \right) \right\rangle , \quad (3)$$

and its frequency spectrum is the dynamic structure factor, $S(q,\omega)$.

Figs. 6–7 depict, for some metals, the obtained AIMD results for $F(q,t)$. The $F(q,t)$ are qualitatively similar for all the metals, namely, for small q's they show a time-dependent oscillatory behavior which becomes weaker with increasing q values and practically disappears at around $\approx(4/5)q_p$. Moreover, these oscillations are superposed on a diffusive component which becomes more marked with increasing atomic number.

The time FT of the $F(q,t)$ gives the associated $S(q,\omega)$, and in Fig. 8 we have plotted them for a range of small q-values where the side-peak is clearly visible. For all the metals studied in this paper, the associated $S(q,\omega)$ show a similar qualitative behavior, namely, the presence of side-peaks, up to $q \approx (3/5)q_p$, which are indicative of the existence of collective density excitations and for greater q-values the $S(q,\omega)$ present a monotonic decreasing behavior.

From the positions of the side-peaks, $\omega_m(q)$, the corresponding dispersion relation of the collective density excitations has been derived, and plotted in Fig. 9. Its slope at $q\to 0$ yields the adiabatic sound velocity, c_s. We have used the values $\omega_m(q)/q \equiv c_s(q)$, within the range $q \leq 1.0$ Å^{-1}, to perform an extrapolation to $q \to 0$ so as to get an approximate estimation for c_s. The obtained values for the adiabatic sound velocity are given in Table 3 where they are compared with the available experimental/semiempirical data. Indeed, l-Mo is the only system for which the c_s has been measured [10] and for which we have obtained a rather good agreement. As for all the other systems, there are only available estimates, obtained from some semi-empirical formulas [36,59] which relate the adiabatic sound velocity with other thermophysical magnitudes such as surface tension, density and melting temperature. We observe a reasonable concordance with the present AIMD calculations with the greater differences appearing for l-Rh and l-Ru. Note that other approaches to estimate the sound velocity from computer simulations are possible (see [40] and references therein), but they
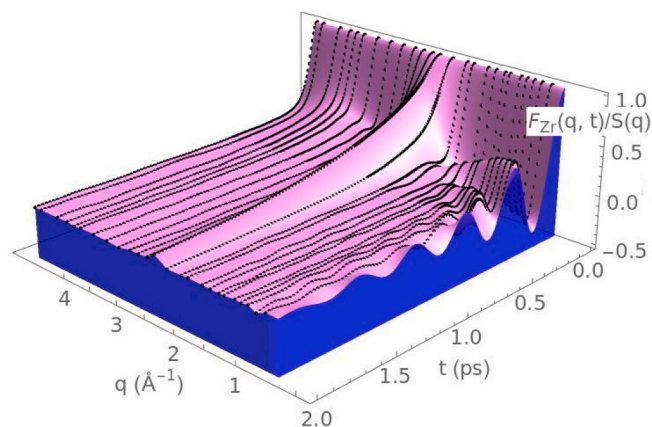

Fig. 6. Intermediate scattering function, $F(q,t)/S(q)$, of l-Zr at $T = 2150$ K for several q values.
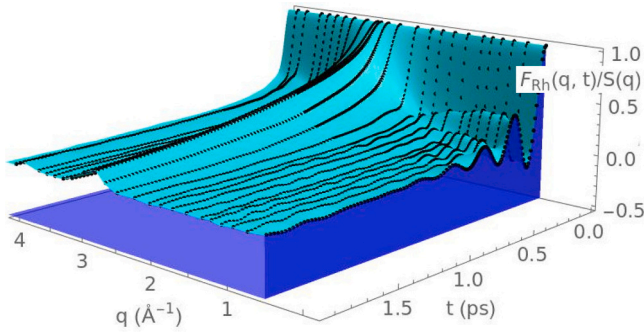
Fig. 7. Intermediate scattering function, $F(q,t)/S(q)$, of l-Rh at $T = 2300$ K for several q values.
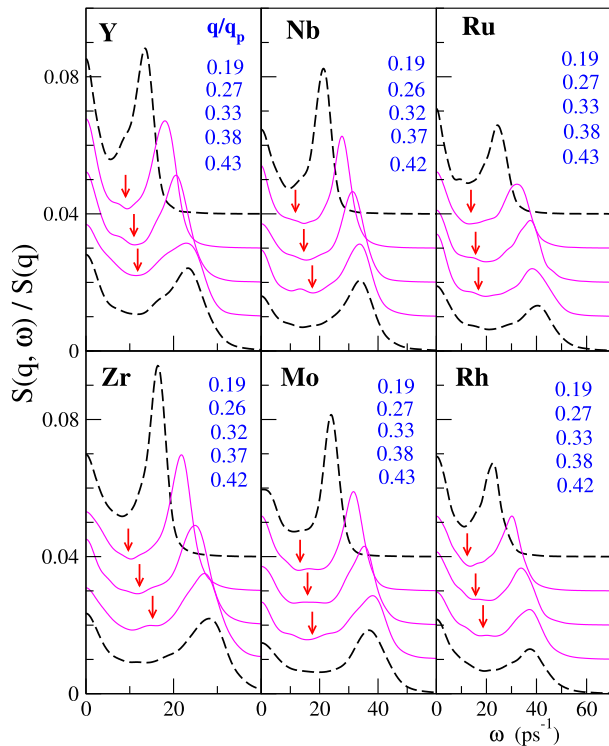

Fig. 8. AIMD calculated dynamic structure factors $S(q,\omega)/S(q)$ for various (top to bottom) q/q_p values. The vertical scales are offset for clarity. The arrows point to the locations of the maxima in the $J_T(q,\omega)$.
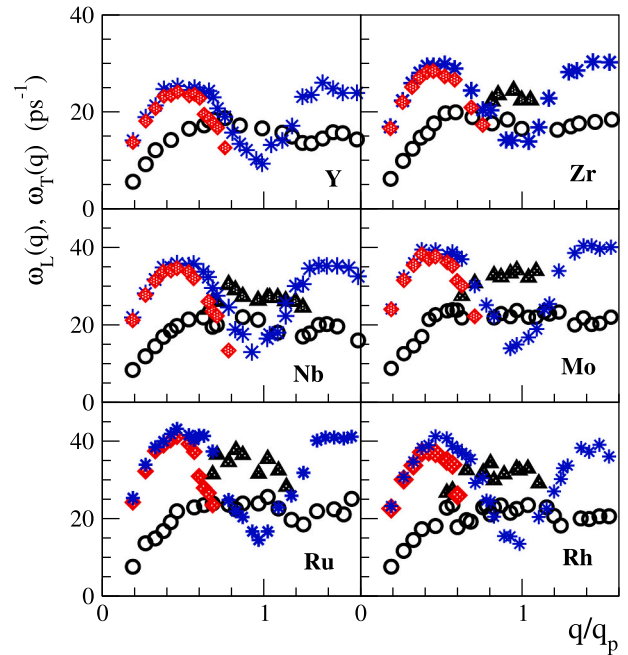

Fig. 9. Dispersion relations for the 4d liquid metals reported in this paper. Red diamonds and blue stars: Longitudinal dispersion obtained from the AIMD results for the positions of the inelastic peaks in the $S(q,\omega)$ and from the maxima in the spectra of the longitudinal current, $J_L(q,\omega)$, respectively. Open circles and triangles: Transverse dispersion from the positions of the peaks in the spectra $J_T(q,\omega)$. (For interpretation of the references to colour in this figure legend, the reader is referred to the web version of this article.)

where $\mathbf{v}_j(t)$ is the velocity of particle j at time t.

The time FT of the $J_L(q,t)$ gives its associated spectra $J_L(q,\omega) = \omega^2 S(q,\omega)/q^2$. From our AIMD results, we have found that for each q-value, the corresponding $J_L(q,\omega)$ shows just one peak and from the frequencies of these peaks, the dispersion relation for the longitudinal modes, $\omega_L(q)$, has been obtained. These curves are also plotted in Fig. 9 where it is observed that they reach their minimum value at the position of the main peak of the corresponding $S(q)$ which is a feature already observed in other liquid metals [41].

Information about the existence of shear modes in the liquid can be gathered from the transverse current correlation function, $J_T(q,t)$, defined as [34]

$$J_T(q,t) = \frac{1}{N}\langle j^x(q,t)\ j^x(-q,0)\rangle \equiv \frac{1}{N}\langle j^y(q,t)\ j^y(-q,0)\rangle . \qquad (6)$$

where $j^x(q,t)$ and $j^y(q,t)$ are the x and y components of $\mathbf{j}(q,t)$ when the z axis is chosen parallel to $\mathbf{q}$. The $J_T(q,t)$, is not associated with any measurable magnitude and can only be determined by means of computer simulations. Its shape evolves from a gaussian, in both q and t, at the free particle ($q \to \infty$) limit, towards a gaussian in q and exponential in t at the hydrodynamic limit ($q \to 0$), *i.e.*

$$J_T(q\to 0,t) = \frac{1}{\beta m}e^{-q^2\eta|t|/m\rho} , \qquad (7)$$

where η is the shear viscosity coefficient. The structure of the $J_T(q,t)$ corresponding to both limiting cases means that it always takes positive values. However, at intermediate q-values it usually shows, within a certain range of q, well-defined oscillations [34,42,43,60]. Indeed, we still lack a theory of transverse dynamics in liquid systems that could

should produce values within the error bars of those reported here, which are mainly dictated by the smallest q-value attainable in the simulations.

Additional information about the density fluctuations can be obtained from the longitudinal current correlation function, $J_L(q,t)$, given by [34].

$$J_L(q,t) = \frac{1}{N}\langle \mathbf{u}_q \cdot \mathbf{j}(q,t)\quad \mathbf{u}_q \cdot \mathbf{j}(-q,0)\rangle \qquad (4)$$

where $\mathbf{u}_q = \mathbf{q}/q$ and $\mathbf{j}(q,t)$ is the FT of the microscopic current defined as

$$\mathbf{j}(q,t) = \sum_{j=1}^{N} \mathbf{v}_j(t)\ exp\left[i\mathbf{q}\cdot\mathbf{R}_j(t)\right] , \qquad (5)$$

explain the structure of the transverse current correlation functions outside the hydrodynamic regime where it has been suggested that there could exist some coupling of the transverse and longitudinal dynamics.

The time FT of the $J_T(q,t)$ gives its spectra $J_T(q,\omega)$ which, when plotted as a function of ω, may display peaks within some q-range, which are related to propagating shear waves. In fact, the lowest q value allowed by the present AIMD simulations, q_{min}, is already outside the hydrodynamic region because the $J_T(q,\omega)$ displays a peak which indicates that propagation of shear waves already takes place at this q_{min}.

In Fig. 10 we have depicted the obtained AIMD results for both $J_L(q,\omega)$ and $J_T(q,\omega)$ at $q/q_p \approx 0.33$. For increasing q-values we obtain that the peaks of $J_T(q,\omega)$ become broader and less marked; moreover, for some metals, we also obtain a second, higher frequency, peak which appears in a narrow range of q-values. From the position of the peaks in the $J_T(q,\omega)$, a dispersion relation for the transverse modes has been obtained and this is plotted, together with the longitudinal dispersion relations, in Fig. 9. Excepting l-Y, we have found that all the other metals exhibit two transverse dispersion branches with the high-frequency one existing over a limited q-range around the position of the main peak of the $S(q)$. The low-frequency transverse branch exhibits the typical behavior found in other liquid metals near melting, namely, this branch starts at a value $q_T > 0$ (which is smaller than the q_{min} of the simulation), smoothly increases up to $q \approx q_p$ where it reaches a maximum and therefrom smoothly decreases and fades away at $q \approx 3.0 \; q_p$. Nevertheless, the most interesting feature is the existence of the high frequency dispersion branch. This feature was first found in some liquid metals at high pressure, *i.e.* Li, Na, Fe, Al and Pb, [19,24,64] and it was assumed that it was a characteristic of high pressure systems. However, recent *ab initio* studies of l-Zn, l-Sn, l-Pb, l-Tl and some liquid 3d transition metals at ambient pressure [22–24,51,31,57] have also found this second high-frequency transverse branch. Moreover, in all these systems this branch appeared only for wave numbers greater than the first pseudo-Brillouin zone boundary, *i.e.*, for $q \geq q_p/2$.

The appearance of two (high- and low frequency) transverse branches has recently been explained in terms of mode-coupling ideas. Specifically, recent studies of l-Zn and l-Sn near melting [22,51] have established a connection between the double mode structure in the $J_T(q,\omega)$ and the coupling of the transverse current with density fluctuations at all wave vectors. On the other hand, we notice that this second branch does not show up in l-Sc and l-Y, which happen to be the metals

with the smallest number density in the 3d and 4d transition groups respectively. So, we tentatively suggest that the important factor that determines the appearance of a high frequency branch in the transverse dispersion relation could in fact be the number density rather than the pressure (although obviously an increase in pressure implies an increase in density).

Recently, del Rio *et al*, based on room pressure results for l-Zn and l-Sn [22,51], suggested that the appearance of a high frequency transverse branch and of two clear maxima in the VDOS, $Z(\omega)$, are closely related. Bryk and coworkers [23,24,64] also found such a relationship in their AIMD studies of l-Tl and pressurized l-Al and l-Pb. The present AIMD simulation results corroborate this connection between the structure of the VDOS and the existence of one/two transverse dispersion branches. Thus, as shown in Figs. 5 and 9, we find that l-Y has a VDOS with one peak and also just one transverse dispersion branch. But for the other 4d metals we observe that the associated VDOS display one peak along with a (higher-frequency) shoulder/peak and the corresponding transverse dispersion show two branches. We note that a similar correlation was found in an AIMD simulation study of several liquid 3d transition metals [31,57]. In principle, such a connection should not come as a surprise because several years ago Gaskell and Miller [44,61,62] had developped, within the framework of the mode-coupling theory, a formulation of the VACF in terms of contributions representing the coupling of the single particle motion to the collective longitudinal and transverse currents. However, we still lack a more detailed account about the precise way these correlations are established.

In the last ten years, much work has been devoted towards the observation and/or calculation of transverse-like low-energy excitations which may show up as weak shoulders in the dynamic structure factor [16,17] and/or the spectra of the longitudinal current [17,18,46]. The first experimental observation was reported by Hosokawa *et al* [16] in an study of l-Ga near melting. They had performed an IXS measurement of the $S(q,\omega)$ and found low energy transverse-like excitation modes showing up shoulders of the quasielastic peak, far below the energy of the longitudinal acoustic modes, which were corrobated by an AIMD simulation study. These excitation modes were attributed to the influence of transverse excitations into the longitudinal dynamics. Afterwards, similar excitation modes were detected, experimentally and in AIMD simulatons, in the $S(q,\omega)$ of several other liquid metals (*i.e.* Fe, Cu, Sn, Ni, Zn) [17,21]. These excitations are usually visible within a small q-range around $q_p/2$, because for smaller/greater q-values they are overcome by the quasielastic/inelastic peaks of the $S(q,\omega)$.

We have analyzed the AIMD simulation results for $S(q,\omega)$ and found that within the range $q/q_p \leq 1/2$ and in the ω-region located between the quasielastic and the inelastic peaks, the $S(q,\omega)$ shows an unusual shape characterized by the appearance of some weak shoulders. This is shown in Fig. 8 where it is also noticed that outside the $q/q_p \leq 1/2$ range, those weak shoulders are no longer visible in the $S(q,\omega)$. Moreover, notice that in the above mentioned ω-region the the energies associated to these shoulders are close to those corresponding to the peaks in the transverse current spectra. Furthermore, as $J_L(q,\omega) = (\omega/q)^2 S(q,\omega)$, these low energy transverse-like excitation modes might also show up in the $J_L(q,\omega)$; therefore, we have plotted together in Fig. 10 both $J_L(q,\omega)$ and $J_T(q,\omega)$. Notice that the $J_L(q,\omega)$ display weak shoulders at frequencies close to those where the $J_T(q,\omega)$ has a peak; moreover, these frequencies are also very close to the frequencies associated with the weak shoulders in their respective $S(q,\omega)$.

The physical origin of these transverse-like excitation modes in liquid metals is still a matter of debate, since no theory has been able to provide an explanation for their appearance yet; nevertheless some alternative interpretations, for instance in terms of heat waves, have been proposed [47].

We consider next the shear viscosity coefficient, η, that has been evaluated from the AIMD results for the $J_T(q,t)$ [42,45,63]. Table 4 presents the obtained results along with the available experimental data. Despite their high melting points and reactivity at high temperatures,
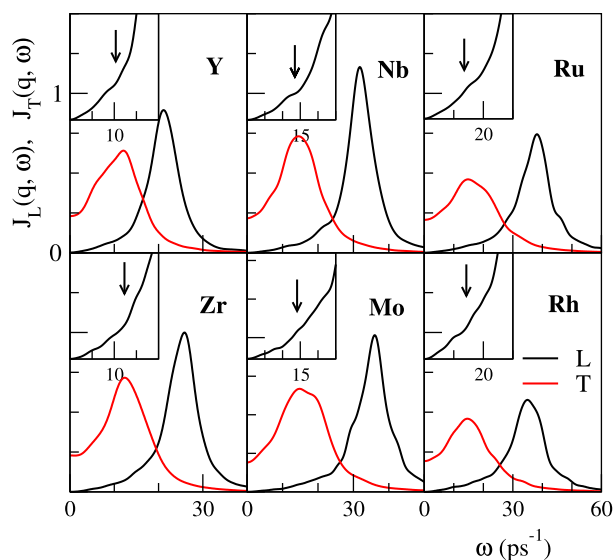

Fig. 10. AIMD calculated longitudinal and transverse currents spectral functions, $J_L(q,\omega)$ and $J_T(q,\omega)$ respectively, for several 4d metals at $q/q_p = 0.33$. The insets in the graphs provide a closer view of the small ω region of the $J_L(q,\omega)$ and the arrows point to the locations of the maxima in $J_T(q,\omega)$.

the viscosities of these 4d liquid metals have been measured by means of levitation techniques [5–8] and an uncertainty of around 10% (20% for l-Y). Those data are listed in Table 3 where we observe a very good accord with the present AIMD calculations.

For l-Zr, we already mentioned that Su *et al* [9] have performed measurements of its viscosity along with its temperature dependence. At thermodynamic conditions near melting, they obtained a value $\eta_{exp} \approx$ 4.50 GPa ps whereas their CMD simulations yielded $\eta_{CMD} \approx 3.50$ GPa ps. They explained this discrepancy in terms of the existence of some oxigen present in the l-Zr sample as the oxigen disolved in l-Zr increases the viscosity. Nevertheless, their experimental value agrees with the data of Ishikawa and Paradis [6] and their CMD simulation result is close to the present AIMD calculation.

Within the context of brownian particles and using purely macroscopic considerations the Stokes-Einstein (SE) relation, $\eta D = k_B T / 2\pi d$, establishes a connection between the self-diffusion coefficient D of a particle with a diameter d moving in a liquid of viscosity η. Surprisingly, it has been found that this relation provides a good empirical correlation when applied to a range of liquid metals; indeed the SE relation has been used to estimate η (or D) by identifying d with the position of the main peak of $g(r)$. In the specific case of MD simulations, as the evaluation of the self-diffusion coefficient takes much less computation time than the calculation of the shear viscosity, then it has become a common practice to use the SE relation to get an estimate of the shear viscosity, once the self-diffusion coefficient has been obtained. Moreover, the SE relation has also been used in the derivation of several semiempirical formulas relating, in terms of other thermophysical magnitudes, the shear viscosity and the self-diffusion coefficient. Now, by using the present AIMD results, we have analyzed the accuracy of this relation when applied to several 3d and 4d liquid transition metals. The results are plotted in Fig. 11 where it is found that, in general, the SE relation still holds fairly well.

3.3. Electronic properties: Density of states

We have also calculated the partial and total electronic density of states, $n(E)$. This has been obtained from the self-consistently determined eigenvalues, and it was averaged over four ionic configurations well separated in time (≈ 15.0 ps), sampling the Brillouin zone with eight k-points.

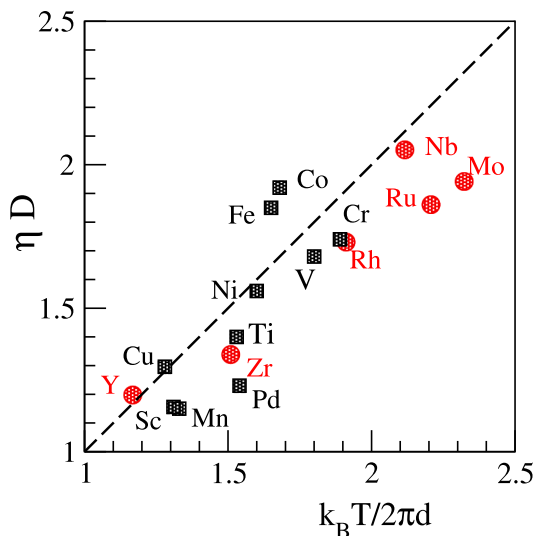Fig. 12 shows the obtained results for the electronic partial and total

Fig. 11. Stokes-Einstein relation. Black squares: 3d metals. Red circles: 4d metals. (For interpretation of the references to colour in this figure legend, the reader is referred to the web version of this article.)
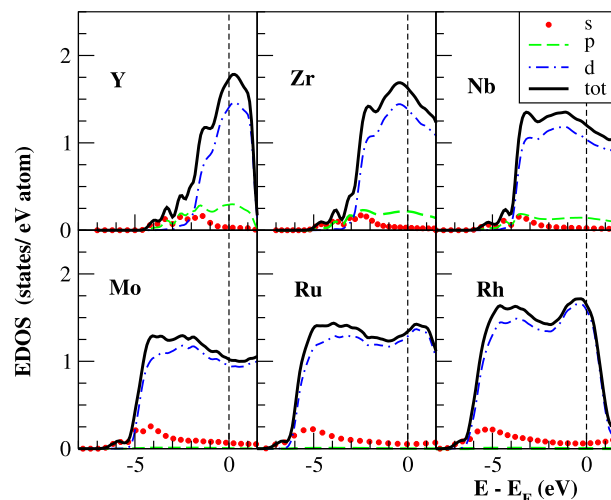
Fig. 12. Total electronic density of states (black line) for several 4d transition metals. The angular momentum decomposition of the DOS in *s* (red dotted line), *p* (green dashed line) and *d* (blue dash-dotted line), (For interpretation of the references to colour in this figure legend, the reader is referred to the web version of this article.)

$n(E)$ associated to the outer valence electrons. The $n(E)$ is dominated by the 4d states, with a very small contribution from the 5s states. In the case of the metals Y, Zr and Nb, there is some contribution from the 4p states but it becomes negligible for Mo, Ru and Rh. In the figure we observe the progresive filling of the d band, together with the increase of its height as the occupation rises.

4. Conclusions

A range of static, dynamic and electronic properties of several liquid 4d transition metals have been calculated by using an *ab initio* simulation method. For most of these metals, this is the first AIMD study performed on them.

The obtained results for the static structure show a very good agreement with the available experimental data in those two metals (l-Zr and l-Rh) for which the comparison can be performed.

The calculated $S(q)$ display an asymmetric shape in its second peak with a marked shoulder (in agreement with the recent XD data). A similar feature has been found in other liquid transition metals and has been related to the appearance of icosahedral short-range order. This latter point has been confirmed by a more detailed study of the liquid static structure by using the CNA method, which has revealed a large abundance of five-fold structures, which are somewhat angle-distorted as compared to ideal icosahedral ones.

As for the single-particle dynamical magnitudes, we have calculated the velocity autocorrelation functions and their associated power spectra, $Z(\omega)$. The obtained $Z(\omega)$ show a peak followed by a more/less noticeable shoulder, excepting l-Y which shows a peak only.

The AIMD dynamic structure factors, $S(q, \omega)$, show side-peaks which are indicative of collective density excitations. Furthermore, we have also found that the $S(q, \omega)$ exhibit some kind of excitations which have similar features as the transverse-like excitation modes found in IXS and INS experimental data for several other liquid metals.

The AIMD transverse current correlation functions, $J_T(q, t)$, exhibit clear oscillations around zero and the associated spectra, $J_T(q, \omega)$, have inelastic peaks which reflect the presence of shear waves. Moreover, we found that these liquid metals (excepting l-Y) exhibit two branches in their associated transverse dispersion relation. Furthermore, these results support the proposed connection between the structure of the VDOS and the existence of one/two transverse dispersion branches.

Several transport coefficients, namely the self-diffusion, adiabatic

sound velocity and shear viscosity coefficients have also been calculated. The obtained results have been used to check the reliability of the Stokes-Einstein relationship when applied to these liquid metals. Given the lack of experimental data for most transport coefficients in these 4d liquid metals and taking into account the reliability of the *ab initio* simulation studies, we expect that the present results will be helpful.

CRediT authorship contribution statement

Declaration of Competing Interest

The authors declare that they have no known competing financial interests or personal relationships that could have appeared to influence the work reported in this paper.

Acknowledgments

References

[1] Y. Waseda, The Structure of Non-Crystalline Materials, McGraw-Hill, New York, 1980.

[2] Y. Waseda, S. Tamaki, The structures of 3d-transition metals in the liquid state, Philos. Mag. 32 (1975) 273.

[3] T. Schenk, D. Holland-Moritz, V. Simonet, R. Bellissent, D.M. Herlach, Icosahedral short-range order in deeply undercooled metallic melts, Phys. Rev. Lett. 89 (2002), 075507.

[4] A. Filipponi, A. di Cicco, G. Aquilanti, M. Minicucci, S. de Panfilis, J. Rybicki, Short-range structure of liquid palladium and rhodium at very high temperatures, J. Non-Cryst. Solids 250-252 (1999) 172.

[5] P.F. Paradis, T. Ishikawa, N. Koike, Thermophysical properties of molten yttrium measured by non-contact techniques, Microgravity Sci. Tec. 21 (2009) 113.

[6] T. Ishikawa, P.F. Paradis, Thermophysical properties of molten refractory metals measured by an electrostatic levitator, J. Electron. Mater. 34 (2005) 1526.

[7] T. Ishikawa, P.F. Paradis, J.T. Okada, Y. Watanabe, Viscosity measurements of molten refractory metals using an electrostatic levitator, Meas. Sci. Technol. 23 (2012), 025305.

[8] T. Ishikawa, P.F. Paradis, J.T. Okada, M.V. Kumar, Y. Watanabe, Viscosity of molten Mo, ta, Os, re, and W measured by electrostatic levitation, J. Chem. Thermodyn. 65 (2013) 1.

[9] Y. Su, M. Mohr, R.K. Wunderlich, X. Wang, Q. Cao, D. Zhang, Y. Yang, H.J. Fecht, J.-Z. Jiang, The relationship between viscosity and local structure in liquid zirconium via electromagnetic levitation and molecular dynamics simulations, J. Mol. Liq. 298 (2020), 111992.

[10] T. Iida, R.I.L. Guthrie, The Thermophysical Properties of Metallic Liquids, Oxford Univ. Press, Oxford, 2015.

[11] N. Jakse, A. Pasturel, Local order of liquid and supercooled zirconium by ab initio molecular dynamics, Phys. Rev. Lett. 91 (2003) 195501.

[12] T.T. Debela, X.D. Wang, Q.P. Cao, D.X. Zhang, S.Y. Wang, C.Z. Wang, J.Z. Jiang, Nucleation driven by orientational order in supercooled niobium as seen via ab initio molecular dynamics, J. Phys. Condens. Matter 26 (2014), 055004.

[13] A.B. Belonoshko, S.I. Simak, A.E. Kochetov, B. Johansson, L. Burakovsky, D. L. Preston, High-pressure melting of molybdenum, Phys. Rev. Lett. 92 (2004), 195701.

[14] D.V. Minakov, M.A. Paramonov, P.R. Levashov, Thermophysical properties of liquid molybdenum in the near-critical region using quantum molecular dynamics, Phys. Rev. B 103 (2021), 184204.

[15] P. Hohenberg, W. Kohn, Inhomogeneous electron gas, Phys. Rev. 136 (1964) B864.

[16] S. Hosokawa, M. Inui, Y. Kajihara, K. Matsuda, T. Ichitsubo, W.C. Pilgrim, H. Sinn, L.E. González, D.J. González, S. Tsutsui, A.Q.R. Baron, Transverse acoustic excitations in liquid Ga, Phys. Rev. Lett. 102 (2009), 105502.

[17] S. Hosokawa, S. Munejiri, M. Inui, Y. Kajihara, W.C. Pilgrim, Y. Ohmasa, T. Sutsui, A.Q.R. Baron, F. Shimojo, K. Hoshino, Transverse excitations in liquid Sn, J. Phys. Condens. Matter 25 (2013), 112101.

[18] S. Hosokawa, M. Inui, Y. Kajihara, T. Sutsui, A.Q.R. Baron, Transverse excitations in liquid Fe, Cu and Zn, J. Phys. Condens. Matter 27 (2015), 194104.

[19] T. Bryk, G. Ruoco, T. Scopigno, A.P. Seitsonen, Pressure-induced emergence of unusually high-frequency transverse excitations in a liquid alkali metal: evidence

[20] of two types of collective excitations contributing to the transverse dynamics at high pressures, J. Chem. Phys. 143 (2015), 104502.

[20] M. Marqués, L.E. González, D.J. González, Structure and dynamics of high-pressure Na close to the melting line: an ab initio molecular dynamics study, Phys. Rev. B 94 (2016), 024204.

[21] B.G. del Rio, D.J. González, L.E. González, Ab initio study of several static and dynamic properties of bulk liquid Ni near melting, J. Chem. Phys. 146 (2017), 034501.

[22] B.G. del Rio, L.E. González, Longitudinal, transverse, and single-particle dynamics in liquid Zn: Ab initio study and theoretical analysis, Phys. Rev. B 95 (2017), 224201.

[23] T. Bryk, T. Demchuk, N. Jakse, J.F. Wax, A search for two types of transverse excitations in liquid polyvalent metals at ambient pressure: an Ab initio molecular dynamics study of collective excitations in liquid Al, Tl, and Ni, Front. Phys. 6 (2018) 00006.

[24] T. Bryk, T. Demchuk, N. Jakse, Atomistic structure and collective dynamics in liquid Pb along the melting line up to 70 GPa: a first-principles molecular dynamics study, Phys. Rev. B 99 (2019) 014201.

[25] P. Gianozzi, et al., QUANTUM ESPRESSO: a modular and open-source software project for quantum simulations of materials, J. Phys. Condens. Matter 21 (2009) 395502.

[26] J.P. Perdew, K. Burke, M. Ernzerhof, Generalized gradient approximation made simple, Phys. Rev. Lett. 77 (1996) 3865.

[27] J.P. Perdew, Y. Wang, Accurate and simple analytic representation of the electron-gas correlation energy, Phys. Rev. B 45 (1992) 13244.

[28] D. Vanderbilt, Soft self-consistent pseudopotentials in a generalized eigenvalue formalism, Phys. Rev. B 41 (1990) 7892.

[29] L. Calderín, D.J. González, L.E. González, J.M. López, Structural, dynamic, and electronic properties of liquid tin: an ab initio molecular dynamics study, J. Chem. Phys. 129 (2008), 194506.

[30] B.G. del Rio, D.J. González, L.E. González, An ab initio study of the structure and atomic transport in bulk liquid Ag and its liquid-vapor interface, Phys. Fluids 28 (2016), 107105.

[31] B.G. Del Rio, C. Pascual, O. Rodríguez, L.E. González, D.J. González, First principles determination of some static and dynamic properties of the liquid 3d transition metals near melting, Condens. Matt. Phys. 23 (2020) 23606.

[32] G.W. Lee, A.K. Gangopadhyay, K.F. Kelton, R.W. Hyers, T.J. Rathz, J.R. Rogers, D. S. Robinson, Difference in icosahedral short-range order in early and late transition metal liquids, Phys. Rev. Lett. 93 (2004), 037802.

[33] Y. Marcus, On the compressibility of liquid metals, J. Chem. Thermodyn. 109 (2017) 11.

[34] U. Balucani, M. Zoppi, Dynamics of the Liquid State, Clarendon, Oxford, 1994.

[35] J.D. Honeycutt, H.C. Andersen, Molecular dynamics study of melting and freezing of small Lennard-Jones clusters, J. Phys. Chem. 91 (1987) 4950.

[36] S. Blairs, Review of data for velocity of sound in pure liquid metals and metalloids, Int. Mater. Rev. 52 (2007) 32.

[37] A.D. Agaev, V.I. Kostikov, V.N. Bobkovskii, Viscosity of liquid refractory metals, Izv. Akad. Nauk. SSSR Met. 3 (1980) 43.

[38] P.F. Paradis, T. Ishikawa, S. Yoda, Thermophysical properties of liquid and supercooled ruthenium measured by noncontact methods, J. Mater. Res. 19 (2004) 590.

[39] O.V. Demidovich, A.A. Zhuchenko, E.L. Dubinin, N.A. Vatolin, A.I. Timofeev, Izv. Akad. Nauk. SSSR Met. 1 (1979) 73.

[40] T. Bryk, G. Ruocco, Generalised hydrodynamic description of the time correlation functions of liquid metals: ab initio molecular dynamics study, Mol. Phys. 111 (2013) 3457.

[41] T. Scopigno, G. Ruocco, F. Sette, Microscopic dynamics in liquid metals: the experimental point of view, Rev. Mod. Phys. 77 (2005) 881.

[42] D.J. González, L.E. González, J.M. López, M.J. Stott, Dynamical properties of liquid Al near melting: an orbital-free molecular dynamics study, Phys. Rev. B 65 (2002), 184201.

[43] J.P. Hansen, I.R. McDonald, Theory of Simple Liquids, Academic Press, London, 1986.

[44] T. Gaskell, S. Miller, Longitudinal modes, transverse modes and velocity correlations in liquids. I, J. Phys. C: Solid St. Phys. 11 (1978) 3749.

[45] B.J. Palmer, Transverse-current autocorrelation-function calculations of the shear viscosity for molecular liquids, Phys. Rev. E 49 (1994) 359.

[46] S. Munejiri, F. Shimojo, K. Hoshino, Static and dynamic structures of liquid tin at high pressure from ab initio molecular dynamics, Phys. Rev. B 86 (2012), 104202.

[47] T. Bryk, J.F. Wax, A search for manifestation of two types of collective excitations in dynamic structure of a liquid metal: Ab initio study of collective excitations in liquid Na, J. Chem. Phys. 144 (2016), 194501.

[48] N. Jakse, O. Le Bacq, A. Pasturel, Short-range order of liquid and undercooled metals: Ab initio molecular dynamics study, J. Non-Cryst. Solids 353 (2007) 3684.

[49] W. Kohn, L.J. Sham, Self-consistent equations including exchange and correlation effects, Phys. Rev. 140 (1965) A1133.

[50] M. Marqués, L.E. González, D.J. González, Pressure-induced changes in structural and dynamic properties of liquid Fe close to the melting line. An ab initio study, J. Phys. Condens. Matter 28 (2016) 075101.

[51] B.G. del Rio, M. Chen, L.E. González, E.A. Carter, Orbital-free density functional theory simulation of collective dynamics coupling in liquid Sn, J. Chem. Phys. 149 (2018), 094504.

[52] P. Gianozzi, et al., Advanced capabilities for materials modelling with Quantum ESPRESSO, J. Phys. Condens. Matter 29 (2017) 465901.

[53] L. Calderín, L.E. González, D.J. González, Ab initio molecular dynamics study of the static, dynamic, and electronic properties of liquid mercury at room temperature, J. Chem. Phys. 130 (2009) 194505.

[54] L. Calderín, L.E. González, D.J. González, Static, dynamic and electronic properties of expanded fluid mercury in the metal–nonmetal transition range. An ab initio study, J. Phys.: Condens. Matter 23 (2011) 375105.

[55] L. Calderín, L.E. González, D.J. González, An ab initio study of the structure and dynamics of bulk liquid Cd and its liquid–vapor interface, J. Phys. Condens. Matter 25 (2013) 065102.

[56] B.G. del Rio, O. Rodríguez, L.E. González, D.J. González, First principles determination of static, dynamic and electronic properties of liquid Ti near melting, Comp. Mat. Sci. 139 (2017) 243.

[57] B.G. Del Rio, L.E. González, D.J. González, Structure and dynamics of the liquid 3d transition metals near melting. An ab initio study, J. Phys. Condens. Matter 32 (2020) 214005.

[58] A.S. Clarke, H. Jónsson, Structural changes accompanying densification of random hard-sphere packings, Phys. Rev. E 47 (1993) 3975.

[59] S. Blairs, Sound velocity of liquid metals and metalloids at the melting temperature, Phys. Chem. Liq. 45 (2007) 399.

[60] J.P. Boon, S. Yip, Molecular Hydrodynamics, Dover, New Yorki, 1991.

[61] T. Gaskell, S. Miller, Longitudinal modes, transverse modes and velocity correlations in liquids: II, J. Phys. C: Solid St. Phys. 11 (1978) 4839.

[62] T. Gaskell, S. Miller, Shear wave modes and velocity correlation spectra in liquids, Phys. Lett. A 66 (1978) 307.

[63] U. Balucani, J.P. Brodholt, P. Jedlovszky, R. Vallauri, Viscosity of liquid water from computer simulations with a polarizable potential model, Phys. Rev. E 62 (2000) 2971.

[64] N. Jakse, T. Bryk, Pressure evolution of transverse collective excitations in liquid Al along the melting line, J. Chem. Phys. 151 (2019), 034506.

[65] B.G. de Rio, O. Rodríguez, L.E. González, D.J. González, First principles determination of static. dynamic and electronic properties of liquid Ti near melting, Comp. Mat. Science 139 (2013) 243.